Applied Thermal Engineering 99 (2016) 1236–1245

Contents lists available at ScienceDirect

Applied Thermal Engineering

journal homepage: www.elsevier.com/locate/apthermeng

Research Paper

Performance simulation of a two-phase flow distributor for plate-fin heat exchanger

P. Yuan [a,b], G.B. Jiang [a], Y.L. He [a], W.Q. Tao [a,*]

[a] Key Laboratory of Thermal Fluid Science and Engineering of MOE, School of Energy and Power Engineering, Xi'an Jiaotong University, Xi'an, Shaanxi 710049, China
[b] School of Energy and Power Engineering, Zhengzhou University of Light Industry, Zhengzhou, He Nan 450002, China

HIGHLIGHTS

- A novel structure of gas–liquid distributor is numerically investigated.
- The results show that the relative flow ratios are usually in the rage of 0.7–1.3.
- The gas side smallest maldistribution is reached when liquid volume fraction is 60%.

GRAPHICAL ABSTRACT

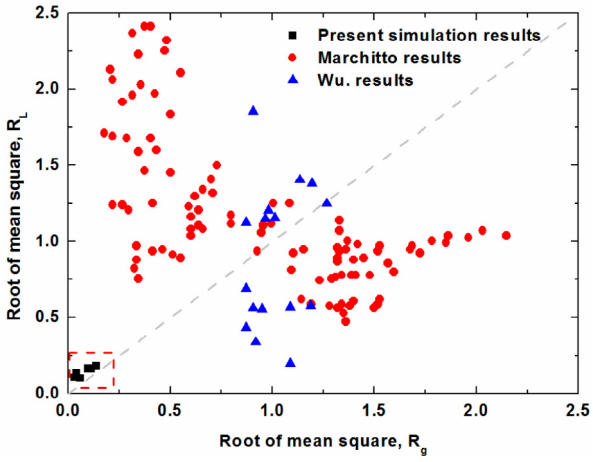

ARTICLE INFO

Article history:
Received 5 November 2015
Accepted 18 January 2016
Available online 29 January 2016

Keywords:
Flow distributor
Heat exchanger
Two-phase flow
Parallel channels

ABSTRACT

Uniform distribution of two-phase flow mixture at the inlet of the plate-fin heat exchanger is critical to the high performance of heat exchanger. Special distributors are often used to improve the distribution. The major purpose of the present paper is to numerically study the distribution characteristics of one type of distributor by using the commercial software CFX. The major feature of this distributor is that ahead of the distributor, gas and liquid separately go into the distributor. Simulations are conducted for air–water mixture. The results reveal that compared with conventional distributors in which ahead of the distributor the fluid is already a two-phase mixture, the proposed distributor can appreciably improve the flow distribution of the plate-fin heat exchanger.

1. Introduction

Plate fin heat exchangers are characterized by high thermal effectiveness, compactness, and ability of heat exchange between many process streams. They are widely used in industrial areas that involve heat transfer, such as air separation, chemical engineering, petroleum refining, and food processing. The heat transfer surface of the plate fin heat exchangers is characterized by multiple channels, and it is essential to uniformly distribute the mass flow rate among the multiple channels for high thermal performance. When designing the plate-fin heat exchangers it is generally assumed that the fluid is uniformly distributed among the multiple channels. However

* Corresponding author. Tel.: +86 029 82669106; fax: +86 029 82669106.
E-mail address: wqtao@mail.xjtu.edu.cn (W.Q. Tao).

http://dx.doi.org/10.1016/j.applthermaleng.2016.01.096
1359-4311/

practically, it is difficult to distribute flow uniformly because of many factors, such as improper arrangement of the inlet configuration and complicated flow structure. Lalot et al. [1] investigated the fluid flow in heat exchanges, and their results indicated that the flow maldistribution leads to an efficiency loss of 25% for cross flow exchangers. The flow maldistribution may be more severe in the case of two-phase flow, and uneven two-phase distribution reduces the thermal performance of compact heat exchangers seriously [2].

In order to overcome the non-uniformity of the flow distribution from the horizontal header toward the channels, some special structures are proposed based on experimental investigation, such as manifold, T-junction or specially-designed distributors. Kitto and Robertson [3] pointed out that numerous factors influence the two-phase maldistribution, such as geometric factors and operating factors. Bernoux et al. [4] experimentally simulated the refrigerant R113 two-phase flow boiling distribution character with the inlet manifold. The results showed that the vapor distribution in channels became more uniform with the increase of the mass quality, but the liquid distribution was not sensitive to the mass flux. Their results show that different phase distribution was in a great extent determined by inlet condition. Vist and Pettersen [2] investigated refrigerant R134a two-phase flow distribution in the manifold with different heat load conditions, and their results show that gas or liquid phase distribution is little affected by the heat load of the evaporator, while two-phase flow distribution influenced the heat transfer greatly. Several authors [5–9] investigated two-phase flow division in T-junctions with multi-outlets and the results showed that T-junctions could not be directly applied to improve the uniformity of flow distribution. Tondeur and Luo [10] proposed a new type of distributor called “constructural distributor” to improve the flow distribution. Due to manufacture imperfection, their experimental result showed 20% flow rate difference. Yue et al. [11] designed a constructural distributor for multi-microchannel based on multiscale shapes and structures theory developed by Bejan [12–14], and got a good uniform stream distribution in high gas flow ratio. Webb and Chung [15] experimentally investigated the two-phase flow distribution character of multiple header-tube junctions applied in heat exchangers, and they concluded that the design of devices to improve flow distribution is “highly empirical”. Because of the flow distribution is influenced by the header orientation (horizontal or vertical), the number of branch tubes, the header shape and tube end projection into the header, and the inlet and exit connection locations have their great effects. Kim and Han [16] also investigated the effect of protrusion depth of the outlet tube of a manifold on the distribution of air–water mixture and found that with the increase in the protrusion depth the flow maldistribution increased. Jiao and Baek [17] proposed adding a complementary empty cavity in the distributor, and they introduced a parameter to define the cavity, which was the ratio of the inlet height to the total height of the distributor. Their experiment results showed that a proper value of this distributor parameter is about 0.22. Ha et al. [18] numerically studied air–water flow distributions character in multi-channels between two headers. They found that the flow distribution uniformity become worse with the increasing of liquid flow rate. Marchitto et al. [19] studied flow maldistribution in multi-parallel channels by fittings installed in the head. Inside the header, through insertion of a co-axial, multi-hole distributor. By the proper selection of position and diameter, their experimental result showed a great improvement of two-phase flow distribution; some similar research has been conducted by [20–22].

Because of the advantages of the Computational Fluid Dynamics (CFD) technique, few works have tried to make out an appropriate model for uniform distribution by CFD. For single-phase flow, Lalot et al. [1] used the code STAR-CD to study the gross flow maldistribution in an electrical heating exchanger. Zhang and Li studied the flow maldistribution in heat exchangers by commercial software FLUENT. Wen and Li [23] studied the flow patterns in the entrance of a plate fin heat exchanger both experimentally and numerically, and they employed software FLUENT and standard $k-\varepsilon$ model to predict turbulent flow. Wang [24] theoretically and numerically investigated the flow distributions in manifolds with FLUENT. Li et al. [25] studied two-phase refrigerant flow in a distributor with multi-manifold branches. The computational results were in quite good agreement with the experiment results. Stevanovic et al. [26] numerically investigated the refrigerant two-phase flow maldistribution from a header with parallel channels in a compact heat exchanger with a computational multi fluid dynamics code. In all the above-mentioned numerical studies the structures of the studied flow distributors are conventional, in which ahead of the distributors the flow media is already a two-phase mixture.

From the above review for both experimental and numerical studies, it can be seen that a great number of investigations on this topic have been carried out, and a lot of methods have been proposed to improve the distribution uniformity, but so far no one can be regarded satisfactory. Among the proposed methods, the flow distributor set up at the inlet of two-phase flow is quite attractive [27]. However, both the geometric structure of the distributor and its practical dimensions need to be further studied. It should be pointed out that the maldistribution of the gas and liquid phases is more evident in compact heat exchangers (such as the plate-fin heat exchangers) than in other types of heat exchangers. So the disadvantage of the gas and liquid two-phase flow maldistribution in the compact heat exchanger should be efficiently overcome for the purpose of improving the heat transfer efficiency.

In the present study, a new structure of two-phase flow distributor introduced in [27] is numerically studied. In the following presentation the structure of the distributor is first introduced. Then the effects of a number of operating conditions on the flow distribution are numerically investigated. The numerically predicted two-phase flow characteristics are compared with authors’ experimental results. Finally, some conclusions are made.

2. Model description and mathematical formulation

A schematic diagram of the plate-fin heat exchanger is shown in Fig. 1a and a cross-section view is shown in Fig. 1b. It is worth noting that the major feature of the plate-fin heat exchanger and the distributor studied in this paper is the separation of liquid and gas phases before they go into the distributor. As shown in Fig. 1b, the gas phase flows into the vertical gas passage ahead of the distributor via the gas inlet, and the liquid phase flows into the crosswise liquid channels of the distributor via the two liquid inlets. It should be noted that illustrated in Fig. 1b is the structure for one unit. It should be pointed out that a plate-fin heat exchanger is consisted of lots of similar units and the identical structure is applied in every unit.

Fig. 2 gives the schematic structure of the distributor. As can be seen from the figure the gas phase and liquid phase channels are connected with a number of cylindrical passages, shown in the plane view by up-and-down small circles. When the plate-fin heat exchanger is in operation, the liquid phase sprays into the gas channels from the liquid channels through these cylindrical passages, finishing primarily mixing with the gas phase. Then, the mixture is distributed into downward small channels. In most conventional distributors the fluid ahead of the distributor is already gas–liquid mixture. Then in the flowing process of the mixture toward the distributor phase separation may occur because of different density of the two phases, often leading to a severe maldistribution of the mixture. The idea that ahead of the distributor gas and liquid are separately supplied can avoid the phase separation problem. Although this idea has been adopted in the plate-fin heat ex-

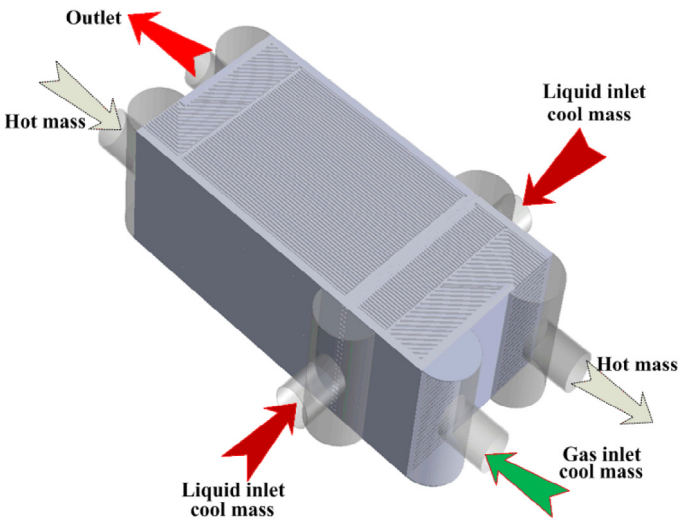

(a) Plate-fin heat exchanger

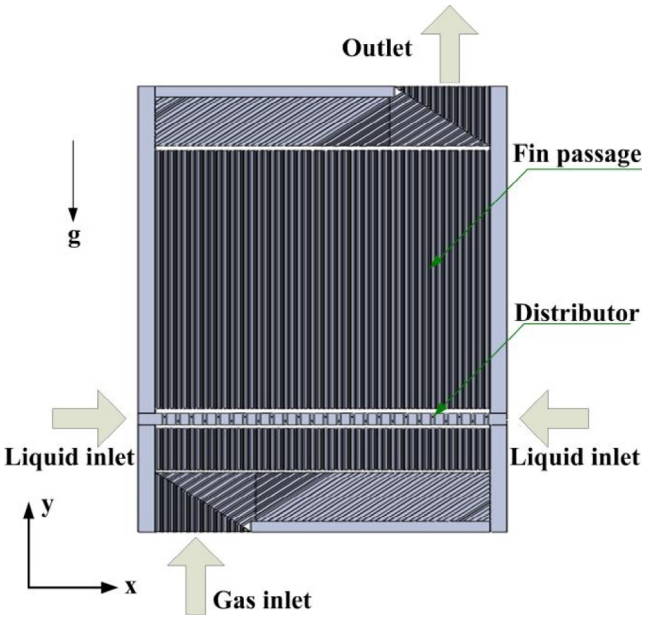

(b) Location of distributor

Fig. 1. PFHE and the distributor.

changer manufacture for a period of time, to our knowledge, only reference [27] experimentally studied the performance of this distributor, and no any numerical investigation has been published in the literature. For the details of the distributor reference [27] may be consulted.

2.1. Simplified physical model for numerical simulation

In an actual plate-and-fin heat exchanger with distributor a small assembly spacing is connected with the distributor and hundreds of channels. To simplify the multichannel structure for numerical simulation, 10 parallel channels are contained in the numerically simulated physical model with the distributor basic structure being the same as a practical case which has a total of 46 cylindrical passages for spraying liquid into gas. Such simplification of multichannel structure was often adopted in literature [28,29]. The computational model is shown in Fig. 3. The gas phase is fed from downward of the distributor along the y plus direction; the liquid phase is from the both ends of the x direction of the distributor. In the downstream after the distributor ten parallel channels are introduced as a simplified multichannel model.

2.2. Mathematical model of the two-phase flow

The commercial CFD software of *ANSYS-CFX* is employed to simulate the two-phase flow. The simulation of the gas–liquid monodispersed flow is based on the Eulerian–Eulerian approach [30], in which the gaseous phase is regarded as continuum and liquid phase as dispersed phase.

To simplify numerical simulation while still keeping the basic characteristics of the process, the following assumptions are made in the present simulations:

(1) The thermal properties of the fluids are constant. The continuous phase is macroscopically regarded as continua, and the dispersed phase is spherical in shape.
(2) For a gas single phase of the inlets, the uniform flow distributions are assumed.
(3) For the two liquid inlets identical flow rates are adopted.
(4) The two-phase flow processes are in steady state and the interfacial mass transfer is not considered.

2.2.1. Continuous phase flow

The standard κ-ε two-equation turbulent model is used to simulate the gas flow in the domain. The scalable wall function is used to simulate the near wall regime. The governing equations for the mass and momentum can be expressed as follows:

The continuity equation:

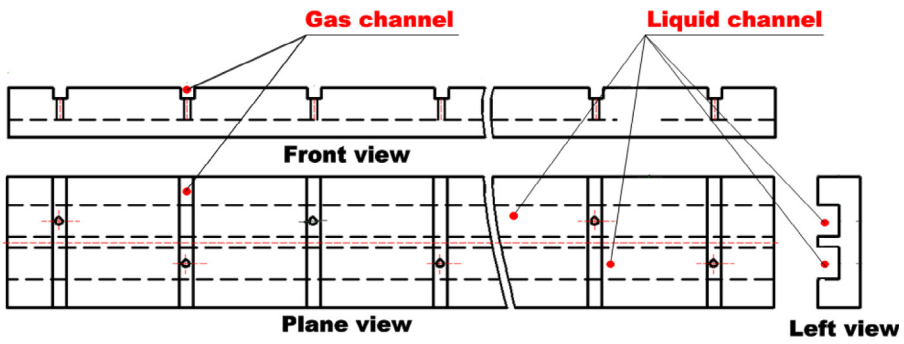

Fig. 2. Structure of the distributor.

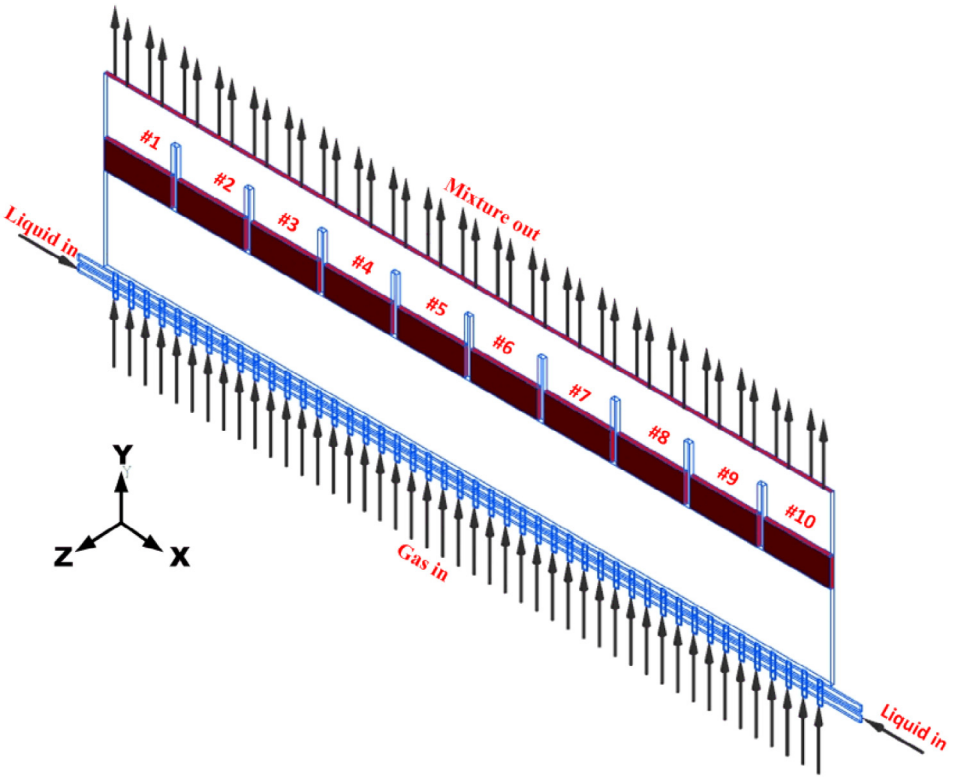

Fig. 3. Schematic drawing of the numerical model.

$$\nabla\cdot(\gamma_\alpha\rho_\alpha U_\alpha)=0 \tag{1}$$

The momentum equation:

$$\nabla\cdot(\gamma_\alpha(\rho_\alpha U_\alpha\otimes U_\alpha))+\gamma_\alpha\nabla P=\nabla\cdot(\gamma_\alpha\eta_{\alpha eff})\left(\nabla U_\alpha+(\nabla U_\alpha)^T\right)+\gamma_\alpha\rho_\alpha g+M_\alpha \tag{2}$$

where U_α is the continuous phase velocity vector, M_α represents the sum of interfacial forces acting on phase α due to the phase β, and $\eta_{\alpha eff}$ is the effective viscosity of the continuous phase. Sato et al. [31,32] suggested that the turbulence stress in the liquid phase of a bubbly flow can be subdivided into two parts, shear turbulence which is independent of the relative motion of the phases and the additional turbulence induced by particles. This idea is borrowed for our study in which gas is the continuum phase and liquid is in particles. So in the present study it is assumed that the effective viscosity of the liquid phase is consisted of three contributions: the molecular viscosity, the turbulent eddy viscosity and an additional viscosity due to the particle induced turbulence, i.e.,

$$\eta_{\alpha eff}=\eta_\alpha+\eta_{t\alpha}+\eta_{td} \tag{3}$$

The turbulent eddy viscosity $\eta_{t\alpha}$ can be expressed by Eq. (4):

$$\eta_{t\alpha}=C_{\eta\alpha}\rho_\alpha\frac{\kappa^2}{\varepsilon} \tag{4}$$

where $C_{\eta\alpha}$ is a constant, and its value is 0.09. When κ-ε model is used to close the stress term, η_{td} is formulated by Eq. (5) proposed by Sato et al. [31]:

$$\eta_{td}=C_{\mu\beta}\rho_\alpha r_\beta d_\beta|U_\beta-U_\alpha| \tag{5}$$

The value of the constant $C_{\mu\beta}$ is equal to 0.6, and d_β is the mean diameter of the disperse phase. The sum of interfacial forces acting on phase α due to the phase β is generally expressed as follows [30]:

$$M_\alpha=M_\alpha^D+M_\alpha^L+M_\alpha^{VM}+M_\alpha^W+M_\alpha^T \tag{6}$$

where the terms of the right hand of Eq. (6) are forces depending on the interphase drag, lift, virtual mass, wall lubrication force and turbulence dispersion, respectively. The drag force per unit volume proposed by Clift et al. [33] can be written as follows:

$$M_\alpha^D=\frac{3}{4}\frac{C_D}{d_\beta}\gamma_\beta\rho_\alpha|U_\beta-U_\alpha|(U_\beta-U_\alpha) \tag{7}$$

The drag coefficient C_D is determined by the empirical correlation from Schiller and Naumann [34,35]:

$$C_D=\frac{24}{\mathrm{Re}_\beta}(1+0.15\mathrm{Re}_\beta^{0.687}) \tag{8}$$

where Re_β is the Reynolds number of the dispersed phase, $\mathrm{Re}_\beta=d_\beta\,|\,U_\beta-U_\alpha\,|\,/\nu_\alpha$, and ν_α is the kinematic viscosity of continuous phase; d_β is the mean diameter.

When a liquid drop travels through other fluids, it is accounted for a lateral lift force perpendicular to the direction of the relative velocity. The force can be correlated to the relative velocity and the local liquid phase velocity from Saffman and Mei et al. [36,37] as

$$M_\alpha^L=\gamma_\beta\rho_\alpha C_L(U_\alpha-U_\beta)\times\nabla\times U_\alpha \tag{9}$$

where coefficient C_L is determined by Eq. (4) in [38], γ_β is volume fraction.

For the steady simulation of the sparsely distributed liquid phase, the virtual mass force and wall lubrication force are relatively smaller and not considered in the study.

Burns et al. [39] and Frank et al. [38] proposed a turbulence force to simulate the random influence of the turbulence eddies. By analogy with molecular movement, the force is found to be

proportional to the local bubble void fraction, with a diffusion coefficient associated with the turbulent kinetic energy. Lopez de Bertodano [40] developed a model to approximate a turbulent dispersion effect for M_α^T, which is given by

$$M_\alpha^T = -C_{TD}\rho_\alpha k_\alpha \nabla\gamma_\alpha \tag{10}$$

where C_{TD} is a non-dimensional empirical constant. The value is in the range of 0.1–0.5 which can give reasonable results for medium sized bubbles in the ellipsoidal particle regime [41,42], k_α is turbulence kinetic energy for phase α. It is noted that the appearance of the turbulence dispersion force is a consequence of the utilization of turbulence modeling used in this work.

The values of κ and ε come directly from the differential transport equation for the turbulence kinetic energy and turbulence dissipation rate, and the interphase transfer for κ and ε is omitted in the equation:

$$\nabla\cdot(\gamma_\alpha\rho_\alpha U_\alpha\kappa) = \nabla\cdot\left[\gamma_\alpha\left(\eta_\alpha + \frac{\eta_{\alpha t}}{\sigma_\kappa}\right)\nabla\kappa\right] + \gamma_\alpha(P_\alpha - \rho_\alpha\varepsilon) \tag{11}$$

$$\nabla\cdot(\gamma_\alpha\rho_\alpha U_\alpha\varepsilon) = \nabla\cdot\left[\left(\eta_\alpha + \frac{\eta_{\alpha t}}{\sigma_\varepsilon}\right)\nabla\varepsilon\right] + \gamma_\alpha\frac{\varepsilon}{\kappa}(C_{\varepsilon 1}P_\alpha - C_{\varepsilon 2}\rho_\alpha\varepsilon) \tag{12}$$

where $C_{\varepsilon 1}$, $C_{\varepsilon 2}$, σ_κ and σ_ε are constants, and their values are 1.44, 1.92, 1.0 and 1.3 respectively. P_α is the turbulence production term due to viscous forces, and its expression is as follows:

$$P_\alpha = \eta_{\alpha t}\nabla U_\alpha\cdot(\nabla U_\alpha + \nabla U_\alpha{}^T) \tag{13}$$

The volume conservation equation can be written as follows:

$$\gamma_\alpha + \gamma_\beta = 1 \tag{14}$$

2.2.2. Dispersed phase flow

The dispersed zero equation models are adopted for dispersed phase turbulent flow. The conservation equations are listed as follows:

The continuity equation:

$$\nabla\cdot(\gamma_\beta\rho_\beta U_\beta) = 0 \tag{15}$$

The momentum equation:

$$\nabla\cdot(\gamma_\beta(\rho_\beta U_\beta\otimes U_\beta)) + \gamma_\beta\nabla P = \nabla(\gamma_\beta(\eta_\beta+\eta_{\beta t}))\left(\nabla U_\beta + (\nabla U_\beta)^T\right) + \gamma_\beta\rho_\beta g + M_\beta \tag{16}$$

where M_β stands for the sum of interfacial forces acting on phase β due to the phases α, such as drag force, lift force, and turbulent dispersion force. The determination of M_β can be conducted as that of M_α presented above.

The additional turbulence dynamic viscosity for the dispersed phase is calculated from the dispersed zero equation model [30,43]:

$$\eta_{\beta t} = \frac{\rho_\beta}{\rho_\alpha}\frac{\eta_{\alpha t}}{\sigma} \tag{17}$$

where the parameter σ is the turbulent Prandtl number relating the dispersed phase kinematic eddy viscosity to the continued phase kinematic eddy viscosity, and its value in the present work is 1 [30].

The governing equations are discretized by the finite volume method [43,44]; the convection term is discretized by 2nd order scheme [45]. The calculations are performed in double precision.

Table 1
Condition of study cases in CFD models.

Case	Liquid inlet velocity (m·s^{-1})	Liquid volume fraction (‰)	Gas inlet velocity (m·s^{-1})
1	5.9	12‰	84.5
2	11.95	24‰	
3	18.14	36‰	
4	24.50	48‰	
5	31.01	60‰	
6	42.25	80‰	

2.3. Simulation condition

The computational domain is divided into a number of discrete control volumes forming a hexahedra mesh. The grid independence test is carried out to ensure a nearly grid independence solution to be obtained. In the test of case 1, three different grid systems with 300,000, 600,000 and 700,000 nodes are adopted for calculation of the whole computational domain. And the difference of the mass flow for liquid and gas in channel 1 between last two node systems is less than 1%. Considering the computational time cost and precisions, 600,000 nodes system is taken for the computation. The properties of working fluids are air and water at 25 °C. Different gas and liquid fractions are investigated in the numerical simulation. Table 1 lists 6 cases studied.

The boundary conditions of the computational domain are set up as follows. The velocity boundary condition is adopted for the gas and liquid inlets. The average static pressure boundary conditions are used for the outlet.

2.4. Convergence criterion

The convergence criterion in the simulation is that the root mean square (RMS) of the variable residuals is lower than 1.0E-04 and the mass flow unbalance between the outlet and inlet is less than 1%. Fig. 4 shows a convergence history of the pressure, and the momentum equations in x and y directions for case 1. It can be seen that after about 350 time steps, the RMS converges to 1.0E-04. When checking the mass flow balance between outlet and inlet 1350 time steps are needed to reach the level of less than 1%. It is worth noting that the iterative solution process in CFX is implemented by transient solution process because of the equivalence between these two

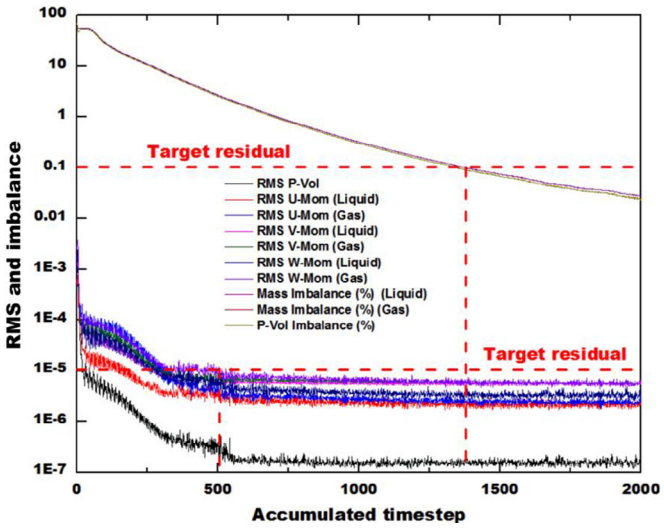

Fig. 4. Convergence history of case 1.

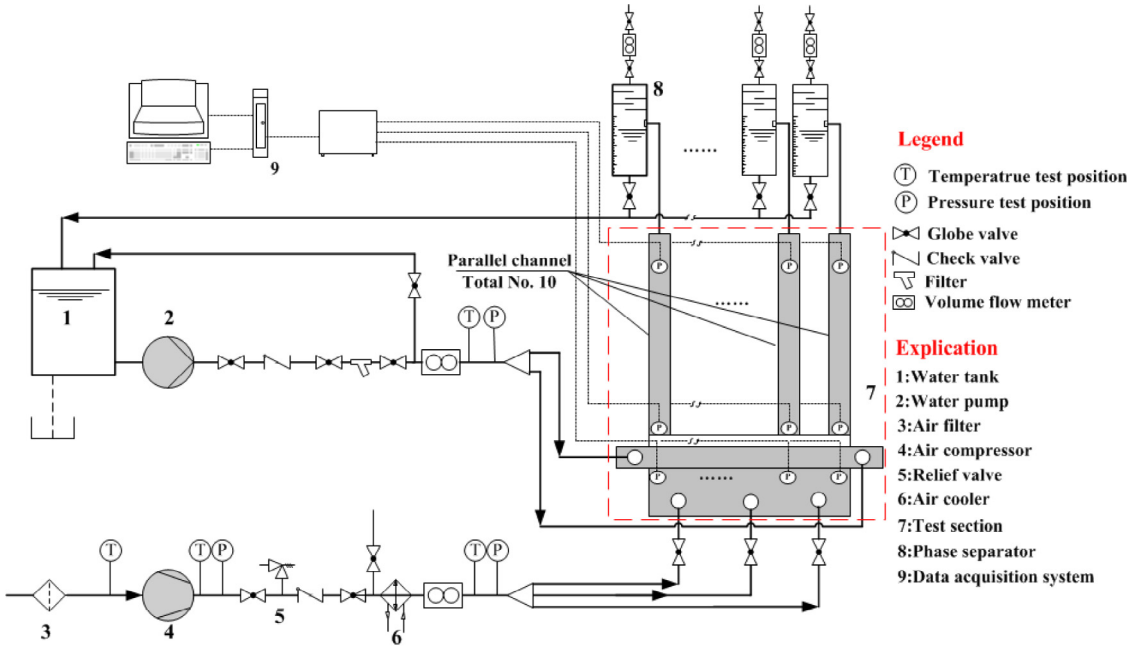

Fig. 5. Schematic of the test facility for the distributor.

processes [43]. Therefore the number of time steps can be regarded as the number of outer iterations.

2.5. The evaluation of flow maldistribution

To investigate the degree of flow maldistribution in the ten channels, the following parameters are introduced:

First, the flow ratio for individual channel is presented in a normalized manner (hereafter, the normalized flow ratio) [2,46,47]:

$$m_{j,t} = \frac{\dot{m}_{j,i}}{\left(\sum_{i=1}^{10}\dot{m}_{j,i}\right)/10} \tag{18}$$

where j = *l* (liquid), or j = g (gas). The value of $m_{j,i}$ reflects the two-phase distribution in channels, and a perfect uniform distribution will lead to 1 of all $m_{j,i}$.

In addition the root mean square of the normalized flow ratio for all the channels is introduced:

$$R_j = \left[\frac{1}{10}\sum_{i=1}^{10}(m_{j,i}-1)^2\right]^{1/2} \tag{19}$$

Obviously, the smaller the value of R_j, the better the flow distribution uniformity.

3. Results and discussion

To validate the computational model and the method adopted in the numerical simulation for the distributor, a corresponding experiment was carried out which covered the gas and liquid velocity range in the computation. Fig. 5 shows the schematic of the test facility. For details reference [27] can be referred.

Fig. 6 shows the gas and liquid distributions of the experimental and simulation results in the ten channels for two different operation conditions, with the inlet condition being given as follows: the gas velocity is 84.5 m s^{-1} for condition 1 and 78.9 m s^{-1} for condition 2; and the liquid phase velocity is 3.26 m s^{-1} and 1.09 m s^{-1} for conditions 1 and 2, respectively.

Fig. 7 exhibits the deviation between the simulated and measured gas and liquid distributions in the ten channels for the two operating conditions. The deviations are calculated as follows:

$$D_j = \frac{(m_{j,i})_{simulation} - (m_{j,i})_{experiment}}{(m_{j,i})_{experiment}} \times 100\% \tag{20}$$

The gas deviation is in the scope of ±8%, and the liquid deviation is in the scope of ±9%. The computational results of the gas and liquid distributions agree with experimental results quite well. The comparison results prove the reliability of the numerical model.

The simulated flow distribution character, expressed by the normalized flow ratio, in 10 parallel channels at different operating conditions is presented in Fig. 8, where x is the total liquid void fraction. The dash line shows the average value, representing the ideal case. The gas normalized flow ratio is in the range of 0.8–1.2, and the liquid is in the range of 0.7–1.3, which shows that the gas flow distribution is more uniform than that of the liquid flow. Observing the trend lines of the normalized flow ratio in channels of gas and liquid phases, the following features may be noted. First, more fluids are centered in the middle channels. The flow rates in Channels No. 1 and No. 10 are lower than the average value, while the flow rate in Channel No. 5 is higher than the average value. Second, with the increase of liquid fraction the liquid flow distribution curve tends to be smoother. Third, the liquid distributions in 10 channels do not change too much when the liquid volume fraction varies from 0.024 to 0.048.

Fig. 9 depicts the effects of the liquid volume fraction on gas and liquid flow distributions in channels with the liquid volume fraction as the abscissa. By increasing the liquid flow ratio, the gas flow distribution uniformity becomes better. When the liquid volume fraction is equal to 60‰, the gas distribution tends to be uniform. This is in good agreement with the corresponding experimental work in [27]. It should be noted that the result is case dependent, and may not be applicable for other type of plate-fin heat exchangers. The maximum gas flow maldistribution occurs near the state of x = 0.24. The same variation characteristics occur in the liquid flow: at x = 0.06 the liquid flow maldistribution is the least, the other two

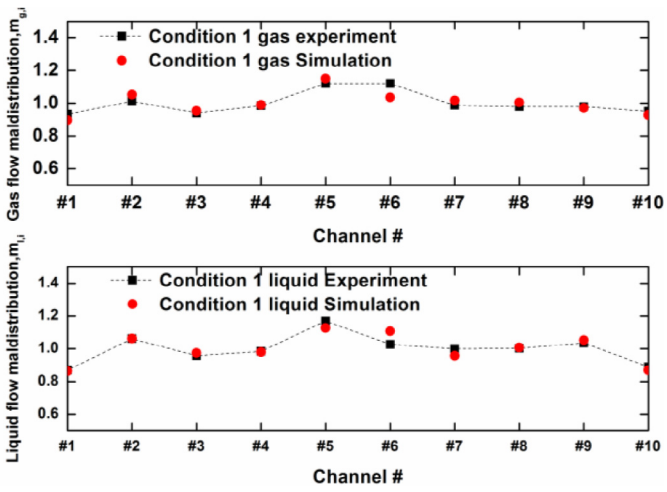

(a) Condition 1

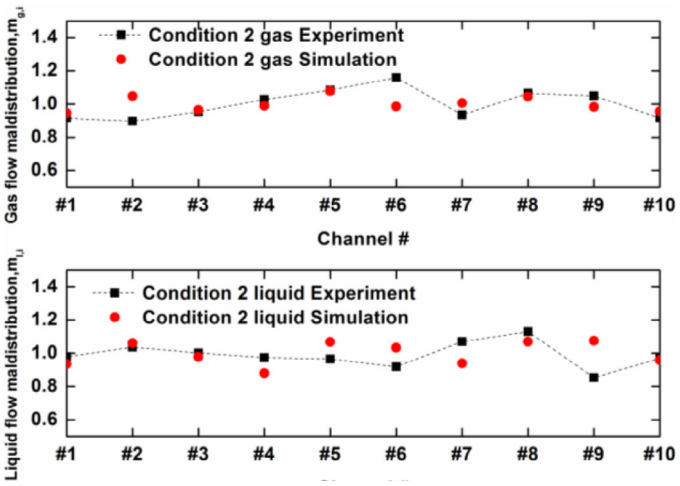

(b) Condition 2

Fig. 6. Comparison between simulation and test results.

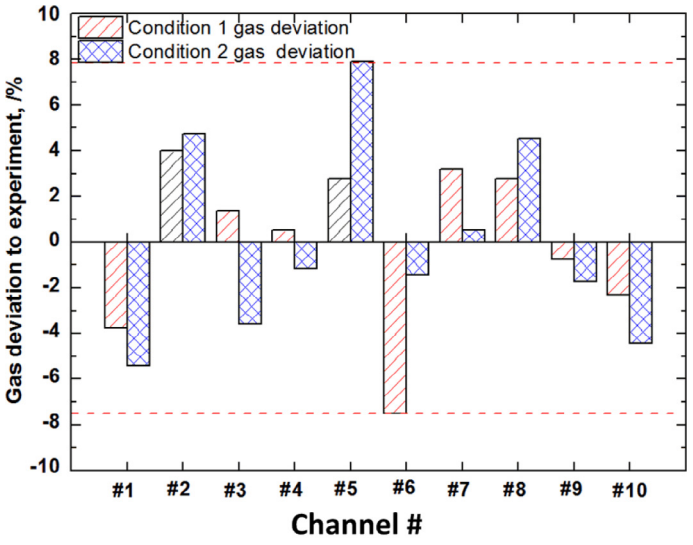

(a) Gas

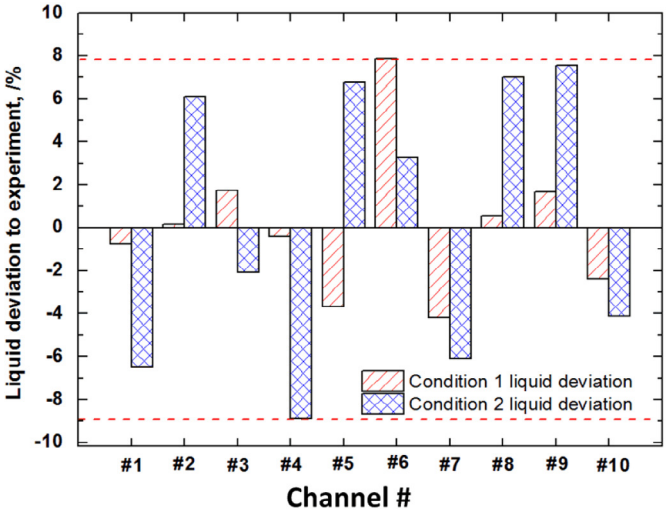

(b) Liquid

Fig. 7. Deviation between simulation and test results.

better states are x = 0.08 and x = 0.012, while when x = 0.024–0.036, the liquid flow maldistribution is the severest.

Fig. 10 indicates the variation of the roots of mean square with the liquid volume fraction. The results show that the gas value is smaller than that of the liquid. The operating condition of x = 0.024–0.048 tends to have severe maldistribution. For the liquid phase x = 0.012 seems to be a better operating condition in the scope of computation conditions.

The liquid mass flow distribution in the 46 cylindrical passages which connect the gas and liquid channels is shown in Fig. 11. It can be seen clearly that the liquid mass flow maldistribution in the cylindrical passages is in the scope of ±10% at different simulation conditions. It may be noted that the flow rate non-uniformity in the cylindrical passages results in the non-uniform spanwise pressure distribution in the assembly, which in turn results in the differences of inlet–outlet pressure drops of the ten channels. It is one of the major reasons leading to the flow maldistribution in the 10 parallel channels (Fig. 8). Further study is needed to improve the distribution uniformity in the cylindrical passages.

Comparisons are made for the numerically predicted root mean square among three kinds of distributors: the present results, the numerical results for flute 180° distributor [19], and that for the head with perforate type distributor [48]. Fig. 12 presents this comparison. It is found that as far as the root mean square is concerned the present distributor exhibits much better performance. The present simulation results are in the left-lower corner shown by the red dash line rectangle. (For interpretation of the references to color in this text, the reader is referred to the web version of this article.) Compared with the results in [19] and [48] not only the values of the root mean square are much smaller, but also the scattering of our data is much less severe than the others.

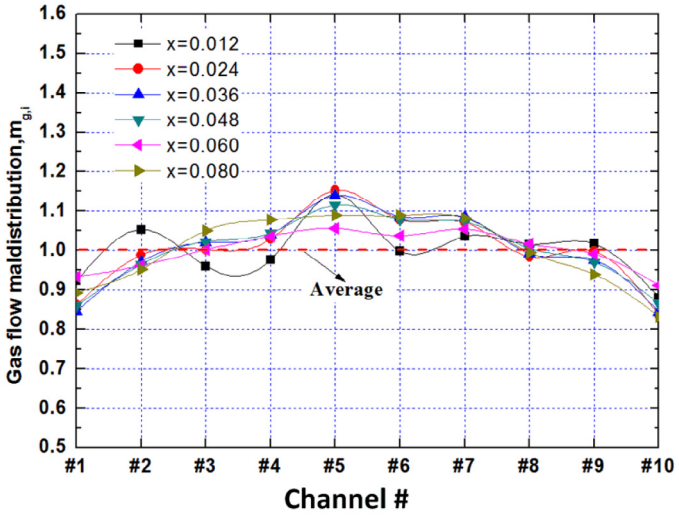

(a) Gas

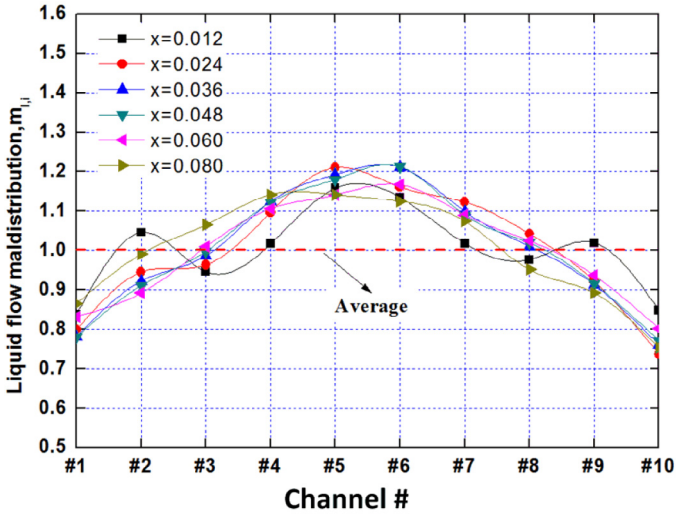

(b) Liquid

Fig. 8. Gas and liquid flow distribution in the channel.

4. Conclusion

In this paper, the gas–liquid distributor with a special structure was numerically investigated using a three dimensional multiphase model with a fixed gas inlet velocity (84.5 m/s) and six liquid inlet velocities (from 5.9 m/s to 42.25 m/s). The flow distributions inside the ten vertical channels for different operating conditions were investigated. The major findings are as follows:

1. The gas normalized flow ratio is in the range of 0.8–1.2, and the liquid one is in the range of 0.7–1.3, which shows that the gas flow distribution is more uniform than that of the liquid flow.
2. Within the cases studied, when the liquid volume fraction is equal to 60‰, the gas maldistribution is the smallest and the gas flow tends to be uniform. The maximum gas flow maldistribution occurs near the state of x = 0.024. For the liquid flow at x = 0.06

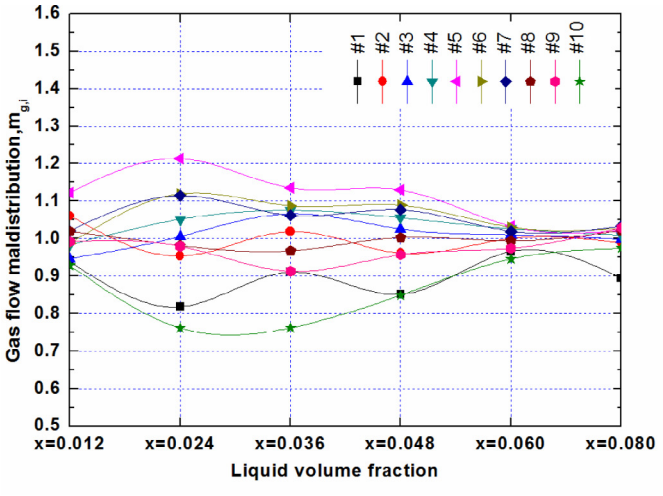

(a) Gas

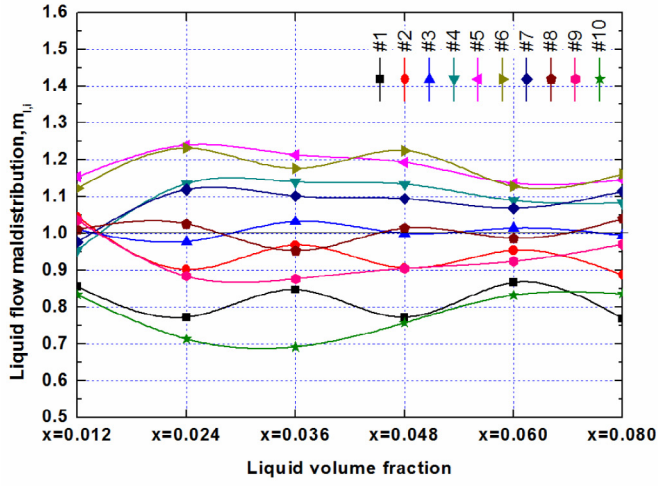

(b) Liquid

Fig. 9. Gas and liquid flow ratios in different states.

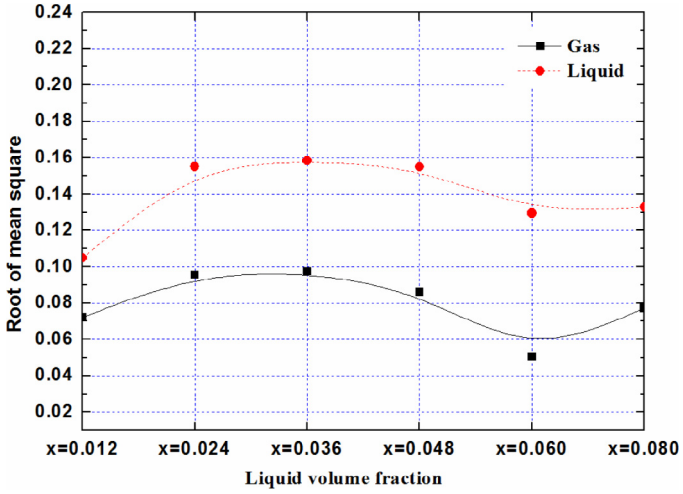

Fig. 10. Root mean square in different operating conditions.

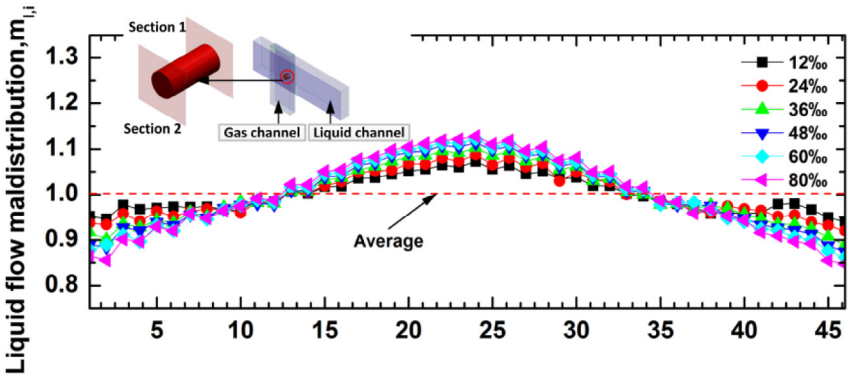

Fig. 11. Normalized liquid flow rate in cylindrical passages.

its maldistribution is the least, while when x = 0.024–0.036, the liquid flow maldistribution is the severest.

3. Compared with the results of other two flow distributors available in literatures the present one has a better distribution performance.
4. The maximum mass flow maldistribution in the 46 cylinder passages which connect the gas and liquid channels is about 10%, which is believed to be one of the reasons leading to the flow maldistribution in the 10 parallel channels.

Acknowledgements

This study was supported by the Emergency Management Project of NSFC (21446011) and the National Key Basic Research Program of China (G2013CB228304).

Nomenclature

U	Velocity vector
C	Empirical constant
R	Root mean square
m	Flow ratio in channel
Re	Reynolds number
d	Mean diameter
γ	Volume fraction
η	Viscosity
κ	Turbulent kinetic energy
ε	Turbulence dissipation rate

Subscripts

α	Continuous phase
eff	Effective viscosity
β	Dispersed phase

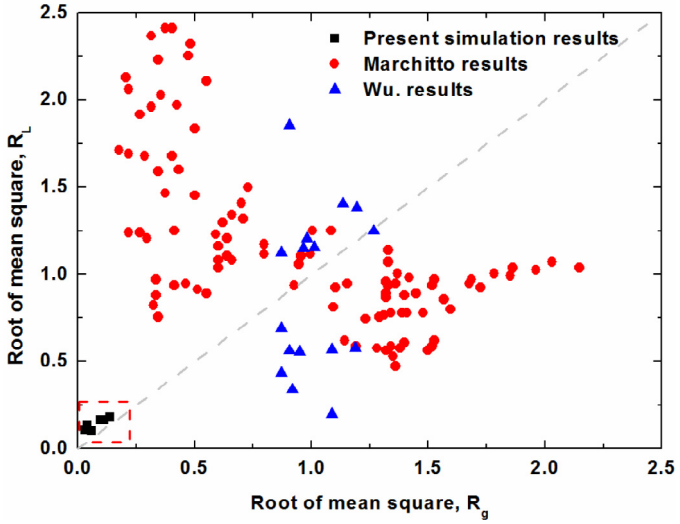

Fig. 12. Comparison of the root mean squares between present simulation and [19,48].

References

[1] S. Lalot, P. Florent, S.K. Lang, A.E. Bergles, Flow maldistribution in heat exchangers, Appl. Therm. Eng. 19 (1999) 847–863.
[2] S. Vist, J. Pettersen, Two-phase flow distribution in compact heat exchanger manifolds, in: 4th International Conference on Compact Heat Exchangers and Enhancement Technology for the Process Industries, Elsevier Science Inc, Grenoble, France, 2004, pp. 209–215.
[3] J. Kitto, J.M. Robertson, Effects of maldistribution of flow on heat transfer equipment performance, Heat Transfer Eng. 10 (1989) 18–25.
[4] P. Bernoux, P. Mercier, M. Lebouche, Two-phase flow distribution in a compact heat exchanger, Compact Heat Exchangers and Enhancement Technology for the Process Industries-2001 (2001) 347–352, 576.
[5] R. Lahey, Current understanding of phase separation mechanisms in branching conduits, Nucl. Eng. Des. 95 (1986) 145–161.
[6] W. Seeger, J. Reimann, U. Muller, Two-phase flow in a T-junction with a horizontal inlet. I: phase separation, Int. J. Multiphas Flow 12 (1986) 575–585.
[7] M. Osakabe, T. Hamada, S. Horiki, Water flow distribution in horizontal header contaminated with bubbles, Int. J. Multiphas Flow 25 (1999) 827–840.
[8] N. Ablanque, C. Oliet, J. Rigola, C.D. Perez-Segarra, A. Oliva, Two-phase flow distribution in multiple parallel tubes, Int. J. Therm. Sci. 49 (2010) 909–921.
[9] T. Hirsch, Use of T junctions as liquid separators in binary flow, Chem Ing Tech 75 (2003) 1856–1859.
[10] D. Tondeur, L.G. Luo, Design and scaling laws of ramified fluid distributors by the constructal approach, Chem. Eng. Sci. 59 (2004) 1799–1813.
[11] J. Yue, R. Boichot, L.G. Luo, Y. Gonthier, G.W. Chen, Q. Yuan, Flow distribution and mass transfer in a parallel microchannel contactor integrated with constructal distributors, AIChE J. 56 (2010) 298–317.
[12] A. Bejan, From heat transfer principles to shape and structure in nature: constructal theory, J. Heat Transfer 122 (2000) 430–449.
[13] A. Bejan, D. Tondeur, Equipartition, optimal allocation, and the constructal approach to predicting organization in nature, Int. J. Therm. Sci. 37 (1998) 165–180.
[14] A. Bejan, Constructal-theory network of conducting paths for cooling a heat generating volume, Int. J. Heat Mass Transf. 40 (1997) 799–816.
[15] R.L. Webb, K. Chung, Two-phase flow distribution to tubes of parallel flow air-cooled heat exchangers, Heat Transfer Eng. 26 (2005) 3–18.
[16] N.H. Kim, S.P. Han, Distribution of air–water annular flow in a header of a parallel flow heat exchanger, Int. J. Heat Mass Transf. 51 (2008) 977–992.
[17] A. Jiao, S. Baek, Effects of distributor configuration on flow maldistribution in plate-fin heat exchangers, Heat Transfer Eng. 26 (2005) 19–25.
[18] M.Y. Ha, C.H. Kim, Y.W. Jung, S.G. Heo, Two-phase flow analysis in multi-channel, J. Mech. Sci. Technol. 20 (2006) 840–848.
[19] A. Marchitto, M. Fossa, G. Guglielmini, Distribution of air–water mixtures in parallel vertical channels as an effect of the header geometry, Exp. Therm. Fluid Sci. 33 (2009) 895–902.
[20] X.F. Guo, Y.L. Fan, L.G. Luo, Multi-channel heat exchanger-reactor using arborescent distributors: a characterization study of fluid distribution, heat exchange performance and exothermic reaction, Energy 69 (2014) 728–741.
[21] H.W. Byun, N.H. Kim, Effect of row-crossing header configuration on refrigerant distribution in a two row/four pass parallel flow minichannel heat exchanger, Int. J. Heat Mass Transf. 89 (2015) 124–137.

[22] H.W. Byun, N.H. Kim, Two-phase refrigerant distribution in an intermediate header of a parallel flow minichannel heat exchanger, Int. J. Refrig. 59 (2015) 14–28.
[23] J. Wen, Y.Z. Li, Study of flow distribution and its improvement on the header of plate-fin heat exchanger, Cryogenics 44 (2004) 823–831.
[24] J. Wang, Theory of flow distribution in manifolds, Chem. Eng. J. 168 (3) (2011) 1331–1345.
[25] G. Li, S. Frankel, J.E. Braun, E.A. Groll, Application of CFD models to two-phase flow in refrigerant distributors, Hvac & R Research 11 (2005) 45–62.
[26] V. Stevanovic, S. Cucuz, W. Carl-Meissner, B. Maslovaric, S. Prica, A numerical investigation of the refrigerant maldistribution from a header towards parallel channels in an evaporator of automotive air conditioning system, Int. J. Heat Mass Transf. 55 (2012) 3335–3343.
[27] P. Yuan, G.B. Jiang, Y.L. He, X.L. Yi, W.Q. Tao, Experimental study on the performance of a novel structure for two-phase flow distribution in parallel vertical channels, Int. J. Multiphas Flow 53 (2013) 65–74.
[28] S.M. Wang, Y.Z. Li, J. Wen, Y.S. Ma, Experimental investigation of header configuration on two-phase flow distribution in plate-fin heat exchanger, Int. Commun. Heat Mass Trans. 37 (2010) 116–120.
[29] Z. Zhang, Y.Z. Li, CFD simulation on inlet configuration of plate-fin heat exchangers, Cryogenics 43 (2003) 673–678.
[30] Ansys-CFX, Ansys-CFX Solver Theory Guide, Ansys Europe, 2010.
[31] Y. Sato, M. Sadatomi, K. Sekoguchi, Momentum and heat transfer in two-phase bubble flow – I. Theory, Int. J. Multiphas Flow 7 (1981) 167–177.
[32] Y. Sato, K. Sekoguchi, Liquid velocity distribution in two-phase bubble flow, Int. J. Multiphas Flow 2 (1975) 79–95.
[33] R. Clift, J.R. Grace, M.E. Weber, Bubbles, Drops, and Particles, Academic Press New York, 1978.
[34] L. Schiller, A. Naumann, über die grundlegenden Berechnungen bei der Schwerkraftaufbereitung, Ver. Deut. Ing 77 (1933) 318.
[35] L. Schiller, Z. Naumann, A drag coefficient correlation, Vdi Zeitung 77 (1935) 318–320.
[36] R. Mei, J. Klausner, Shear lift force on spherical bubbles, Int. J. Heat Fluid Fl. 15 (1994) 62–65.
[37] P.G. Saffman, The lift on a small sphere in a slow shear flow, J. Fluid Mech. 22 (1965) 385–400.
[38] T. Frank, J. Shi, A. Burns, Validation of Eulerian multiphase flow models for nuclear reactor safety applications, 3rd TPFMI, Pisa, 22–24, 2004.
[39] A.D. Burns, T. Frank, I. Hamill, J.M. Shi, The Favre averaged drag model for turbulent dispersion in Eulerian multi-phase flows, in, Vol. 4, 2004.
[40] M. Lopez de Bertodano, Turbulent bubbly flow in a triangular duct, in: Rensselaer Polytechnic Institute, Troy New York, 1991.
[41] M. Lopez de Bertodano, R. Lahey Jr., O. Jones, Development of a k-e model for bubbly two-phase flow, J. Fluids Eng. 116 (1994) 128.
[42] M. Lopez de Bertodano, R. Lahey Jr., O. Jones, Phase distribution in bubbly two-phase flow in vertical ducts, Int. J. Multiphas Flow 20 (1994) 805–818.
[43] W.Q. Tao, Numerical Heat Transfer, Xi'an Jiaotong University Press, Xi'an, China, 2001.
[44] S.V. Patankar, Numerical Heat Transfer and Fluid Flow, Taylor & Francis, 1980.
[45] T.J. Barth, D.C. Jespersen, The design and application of upwind schemes on unstructured meshes, in, Vol. 89, 1989.
[46] A. Marchitto, F. Devia, M. Fossa, G. Guglielmini, C. Schenone, Experiments on two-phase flow distribution inside parallel channels of compact heat exchangers, Int. J. Multiphas Flow 34 (2008) 128–144.
[47] P. Fei, Adiabatic Developing Two-Phase Refrigerant Flow in Manifolds of Heat Exchangers, University of Illinois, Urbana Champaign, 2003.
[48] Y. Wu, T. Wu, L. Chen, New progress in researches on gas-liquid uniform distribution characteristic and typical structure design of cryogenic plate-fin heat exchangers, J. Xi'an Jiaotong Uni. 41 (2007) 383–388.